PCCP

PAPER

View Article Online
View Journal | View Issue

Cite this: *Phys. Chem. Chem. Phys.*, 2021, **23**, 20567

Improving persistent luminescence in pressure-tuned $CsPbBr_3$ nanocrystals by Ce^{3+} doping

Meng Tian, [a] Yang Gao,[b] Pengyu Zhou,[c] Kailin Chi,[c] Yu Zhang[c] and Bao Liu *[ac]

Received 24th June 2021,
Accepted 22nd August 2021

DOI: 10.1039/d1cp02864b

rsc.li/pccp

The pressure-dependent photoluminescence kinetics of $CsPbBr_3$:Ce quantum dots was investigated by steady-state and time-resolved photoluminescence spectroscopy. Here, we propose a novel strategy to improve the persistent luminescence of $CsPbBr_3$ quantum dots under high pressure through doping of Ce^{3+} ions. Under high pressure, the peak intensity and energy of $CsPbBr_3$:Ce quantum dots decreased more slowly than those of $CsPbBr_3$ quantum dots, which is manifested by pressure coefficient reductions of 0.08 a.u. GPa^{-1} and 0.012 eV GPa^{-1}, respectively. The time-resolved photoluminescence measurements revealed that Ce^{3+}-doping can significantly modulate the photoluminescence kinetics to shorten the lifetimes of $CsPbBr_3$ quantum dots with increasing pressure. These phenomena were absolutely different from those observed in $CsPbBr_3$ quantum dots. These findings will be useful for broadening the application of optical devices based on all-inorganic perovskite materials under high pressure.

1. Introduction

Comparing with perovskite films and nanotubes, the size confinement effect of the perovskite quantum dot (QD) spectrum has a narrow emission bandwidth and ideal color purity.[1] The abundant surface effects and element substitution of QDs make the band-gap of perovskites adjustable and the photoluminescence quantum yield (PLQY) higher.[2] With this finding, the external quantum efficiency of halogen perovskite quantum dots has increased to above 20% in green and red emission LED devices and over 12% in blue-ray emission devices within a few years.[3] Furthermore, inorganic perovskite quantum dots (IPQDs) with high formation energies and inherent defect tolerance have drawn tremendous attention in the fields of LEDs,[4] lasers,[5] solar cells,[6] and photodetectors[7] in the recent years. However, large-scale manufacture of IPQDs is limited due to the structural instability of these materials and the unremovable presence of the heavy-metal lead after synthesis. These issues are the crucial challenges for the application of IPQD-based photoelectric devices in industry.

One promising solution to addressing these challenges is the substitution of the lead atoms of $CsPbX_3$ QDs. Partial substitution of the lead atoms will adjust the spectral bandgaps, enhance the phase stability, and reduce the lead levels while retaining both the crystal type and high PLQY of $CsPbX_3$ QDs. Recent studies have demonstrated successful B-site partial doping using divalent dopants (Sn^{2+}, Eu^{2+}, Mn^{2+})[8–10] and trivalent dopants (Yb^{3+}, Ce^{3+}, Tb^{3+}, Er^{3+}, Nd^{3+}).[11–15] For example, Stam *et al.* reported that divalent dopants lead to a blue-shift of the photoluminescence (PL) while retaining the crystal type, high PLQY, and narrow emission bandwidth of the host $CsPbBr_3$ QDs;[16] Zhao *et al.* reported that the surface defect density of $CsPbBr_{1.5}Cl_{1.5}$ QDs may be reduced by Yb^{3+} ion doping, which results in enhanced visible luminescence performance.[17] Despite these advantages, dopants may also lead to negative effects on the physical properties of QDs, for example, the M^{2+} doping products are unstable due to the oxidation of doping ions;[18] the M^{3+} (Nd^{3+}, Bi^{3+}, Yb^{3+}, Er^{3+}, Eu^{3+}) doping with the appearance of dual emission can cause an emission quenching effect due to the formation of defect states in the band gap.[17] Due to these complex effects of partial doping on perovskites, a comprehensive understanding of the impacts of partial doping on the structure and physical properties of perovskites is an urgent necessity. Recent investigations have reported that the Ce^{3+} dopant can significantly modulate the PL kinetics of the $CsPbBr_3$ host without introducing additional defect states.[19,20] This arousing finding has inspired us to investigate Ce^{3+} doping in QDs for potential guided improvements in the properties of perovskites.

High-pressure technology allows clean, efficient and precise regulation of crystal structure and electronic configuration for

[a] *College of Chemical Engineering, Northeast Electric Power University, Jilin, 132012, China. E-mail: liubao@neepu.edu.cn; Tel: +86-(0)432-6480-6621*
[b] *Center for High Pressure Science and Technology Advanced Research, Shanghai 201203, China*
[c] *College of Science, Northeast Electric Power University, Jilin, 132012, China*

the adjustment of the photoelectric properties of materials.[21] An understanding of the variation of pressure induced PL properties provides a promising direction for future practical applications of halide perovskites. In recent years, a variety of novel properties of halide perovskites under pressure have been extensively studied, including pressure-induced emission,[22] structural phase transition,[23] metallization,[24] and amorphization.[25] Among them, the pressure induced linear shift and abnormal evolutions of the PL peak may be attributed to the contraction of the bond lengths and the distortion of the crystal structures. Under high pressure, the unique geometrical morphology effects will induce different phase transition pressures for $CsPbBr_3$ QDs, nanowires, and the corresponding bulk counterparts. The pressure-dependent PL spectra of $CsPbBr_3$ QDs indicated a shorter pressure interval of structural phase transition ($\sim$0.26 GPa) compared with other crystal morphology. With further elevation of pressure, $CsPbBr_3$ QDs show a red-shift in emissions, and PL quenching occurred until the emission became totally undetectable at a pressure of $\sim$1.3 GPa, which is ascribed to pressure-induced amorphization and occurred at a lower pressure compared to its corresponding bulk $CsPbBr_3$ ($\sim$1.85 GPa).[26] All these studies suggest that, when ions are doped into $CsPbBr_3$, pressure is also a powerful controlling factor tuning the PL properties as well. So far, little is known about how pressure affects the PL properties of lanthanide ion doping in $CsPbBr_3$ QDs. Thus, the high-pressure technique and Ce^{3+} doping were conducted on $CsPbBr_3$ QDs to investigate the effect of pressure on the PL properties of $CsPbBr_3$:Ce QDs and reveal the mechanism of its luminescence under pressure.

Here, we investigated the PL kinetics of $CsPbBr_3$:Ce QDs at a high pressure using steady-state and time-resolved photoluminescence (TRPL) spectroscopy with a diamond anvil cell (DAC). The TRPL decay curves of $CsPbBr_3$:Ce QDs at various pressures were recorded to characterize their PL lifetimes, which was found to decrease linearly with pressure elevation. The PL intensities of the $CsPbBr_3$:Ce QDs, on the other hand, decreased at a lower rate than those of undoped ones with pressure elevation. Furthermore, the quenched pressure of the luminescence of $CsPbBr_3$ QDs is enhanced to 2.25 GPa by Ce^{3+} doping compared to that below 1.36 GPa of the original sample. The persistence of luminescence under pressure was increased by 65.4%, which clearly demonstrates the enhancement effects of pressure on the optical properties of $CsPbBr_3$ QDs.

2. Experimental section

2.1 Synthesis and characterization of $CsPbBr_3$:Ce QDs

The targeted $CsPbBr_3$:Ce QDs were synthesized according to the modulated colloidal chemistry method. Cesium carbonate (0.814 g, Cs_2CO_3, Momordicin, 99%), octadecene (40 mL, ODE, Momordicin, 90%), and oleic acid (2.5 mL, OA, 99%, Macklin) were loaded into a 100 mL flask and dried under vacuum at 120 °C for 1 h. The solvent was then heated to 150 °C in a heating oven until Cs_2CO_3 fully reacts with OA. Cs-oleate was preheated to dissolve at 120 °C before use. Subsequently, bromide lead (0.069 g, $PbBr_2$, 99.999%, Macklin) and 5 mL ODE were loaded into a 25 mL flask and dried under vacuum at 120 °C for 1 h. Cerium(III) bromide (0.0214 g, $CeBr_3$, 99.9%, Macklin) and 0.5 ml OA were loaded into a 10 mL flask and heated under vacuum to 60 °C until $CeBr_3$ is fully dissolved. Then 0.5 mL cerium precursor and oleylamine (0.5 mL, OAm, 80–90%, Macklin) were injected into lead precursor solution to form a mixed solution under ambient conditions. Then the temperature was raised to 180 °C until $PbBr_2$ is fully dissolved. After 5 minutes of heating, 0.4 mL Cs–oleate solution was quickly injected. About 60 s later, the reaction mixture was extracted and quenched in an ice-water bath. The resultant mixture was isolated in hexane by centrifuging for 10 minutes at 12 000 rpm. The sample was characterized by transmission electron microscopy (TEM), high resolution TEM (HRTEM), high-angle annular dark-field scanning transmission electron microscopy (HAADF–STEM), and energy dispersive X-ray spectroscopy (EDS) on a JEOL JEM-2100 Plus TEM with an accelerating voltage of 200 kV. The structure of the resulting sample was characterized by X-ray diffraction (XRD) (DX-2700B, Haoyuan Instrument) with Cu-Kα radiation operated at 40 kV and 30 mA, with λ = 1.540598 Å, 0.02° steps and 1 s time/step under ambient conditions.

2.2 *In situ* optical measurements under high pressure

High pressure is generated in a DAC with an anvil culet size of 400 μm in diameter. A sheet of T-301 stainless steel was used as a gasket and indented to 50 μm in thickness before use. A 150 μm diameter hole was drilled at the center of the indentation as the sample chamber. $CsPbBr_3$:Ce QDs and a ruby sphere were loaded into the sample chamber side by side. Silicone oil was used as the pressure-transmitting medium. The high-pressure PL spectra were obtained using a pulsed diode laser with a CW triggered 454 nm laser as the excitation source, and the spectral signal from the 300 g grating was analyzed using a 0.5 m focal length monochromator (SpectraPro HRS-500, Princeton Instruments) with a Peltier-cooled silicon charge-coupled device (PIX-400, Princeton Instruments). The wavelength of the test range of the PL spectrum is 400–600 nm. For TRPL measurements under pressure, the excitation source was changed into pulse triggered mode with a width of 68 ps and a repetition frequency of 10 MHz. The luminescence from QDs was analyzed using a silicon APD. The silicon APD output was then input into a Stand Alone TCSPC Module (PicoHarp 300) for analysis.

3. Results and discussion

The morphology and structure of the synthesized $CsPbBr_3$:Ce QDs were analyzed using TEM and HRTEM characterization. As shown in Fig. 1(a), the $CsPbBr_3$:Ce QDs obtained at a Ce/Pb atomic ratio of 0.0288 show a cubic morphology with an average diameter of 11 $\pm$ 1 nm. The HRTEM image (Fig. 1(a) inset) shows lattice fringes with a *d*-spacing of 0.42 nm which

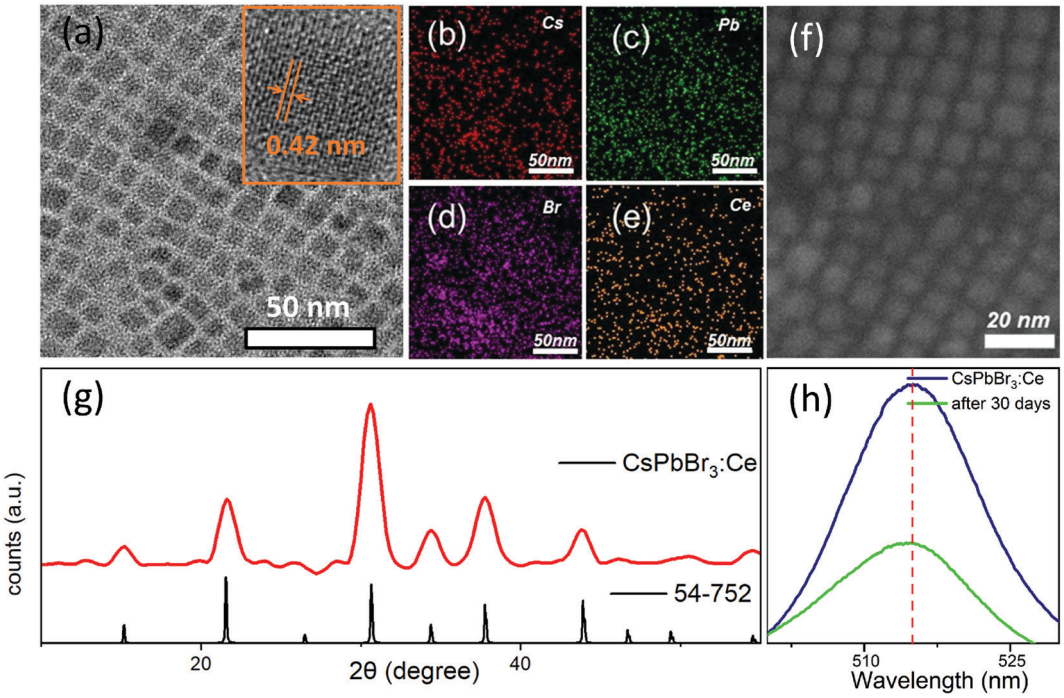

Fig. 1 (a) TEM images of $CsPbBr_3$:Ce QDs and their corresponding HRTEM images in the insets. Elemental mapping of (b) Cs, (c) Pb, (d) Br and (e) Ce elements in the $CsPbBr_3$:Ce QDs. (f) The HAADF-STEM image of $CsPbBr_3$:Ce QDs. (g) XRD pattern of the $CsPbBr_3$:Ce sample (red line) and the XRD pattern of $CsPbBr_3$ (black line). (h) PL spectra of $CsPbBr_3$:Ce QDs and the spectra of $CsPbBr_3$:Ce QDs under ambient conditions after 30 days of exposure to air.

corresponds to the $CsPbBr_3$:Ce QDs (010) planes. The EDS mapping images (Fig. 1(b)–(e)) of the sample show that Cs, Pb, Br, and Ce atoms are evenly distributed throughout the sample, which suggests the existence of Ce^{3+} in QDs in our experimental object. It has been reported that the lanthanide ions would tend to occupy the location of Pb and thus have the lowest formation energy regardless of the concentration of Pb element.[27] The HAADF-STEM image of $CsPbBr_3$:Ce QDs in Fig. 1(f) shows the uniform cubic shape of the resulting products. The XRD pattern in Fig. 1(g) shows that the $CsPbBr_3$:Ce QDs have the same cubic crystalline structure (PDF#54-752) as $CsPbBr_3$ QDs, which indicates that the Ce^{3+}-doping does not change the crystalline structure of $CsPbBr_3$ QDs. The optical properties of $CsPbBr_3$:Ce QDs were investigated *via* PL emission spectroscopy under ambient conditions as shown in Fig. 1(h). The PL emission spectrum shows a peak position at 516 nm (2.41 eV) with a peak width at half height of 16.86 nm. The PL intensity of the $CsPbBr_3$:Ce QDs diminished gradually with time but showed no sudden changes within 30 days, as reported by Zou *et al.*, where the $CsPbBr_3$ QDs undergo a striking degradation and become non-luminous within 30 days under ambient conditions and exposure to air.[28] In this study, after aging in hexane for 30 days without separation from oxygen and moisture, ~50% of the PL peak intensity of $CsPbBr_3$:Ce QDs can be retained, indicating the improved stability of QDs due to the lattice contraction induced by Ce^{3+}-doping.

Considering the outstanding optical properties of $CsPbBr_3$:Ce QDs, we traced the pressure-induced optical evolution *via* high-pressure PL experiments. Selected steady-state PL spectra with increasing pressure and optical micrographs of $CsPbBr_3$:Ce QDs in the sample chamber are shown in Fig. 2(a) and (b), respectively. The PL peaks displayed a red-shift at wavelengths below 1.47 GPa; after that pressure point, an abnormal stark blue jumping appeared. With further pressure elevation, the fluorescence was completely quenched at 2.25 GPa, which may be ascribed to the pressure-induced amorphization. The bulk $CsPbBr_3$ and its corresponding QDs experienced pressure induced amorphization combined with fluorescence quenching phenomena[23] and the PL quenching pressures are 1.85 GPa and 1.36 GPa, respectively.[26] Wisser *et al.* reported that the lanthanide ion doping does not change the pressure induced structure transition sequence, except for affecting the transition pressure.[29] Therefore, we speculated that the pressure induced amorphization would occur on $CsPbBr_3$:Ce QDs as undoped ones, to which the PL quenching phenomenon of $CsPbBr_3$:Ce QDs may be ascribed. The observed quenching pressure of $CsPbBr_3$:Ce QDs was 2.25 GPa, which is higher than that of $CsPbBr_3$ QDs at 1.36 GPa. The full width at half maximum of the PL peak becomes broader with increasing pressure owing to the changes of the band structure under pressure.[30] In Fig. 2(b), the $CsPbBr_3$:Ce QDs were orange in the beginning, faded, and eventually became colorless with pressure elevation up to 2.25 GPa. The observed piezochromism is in accordance with the evolution of PL spectra under pressure. The wavelength of the PL peak was recovered upon decompression from 519 nm at

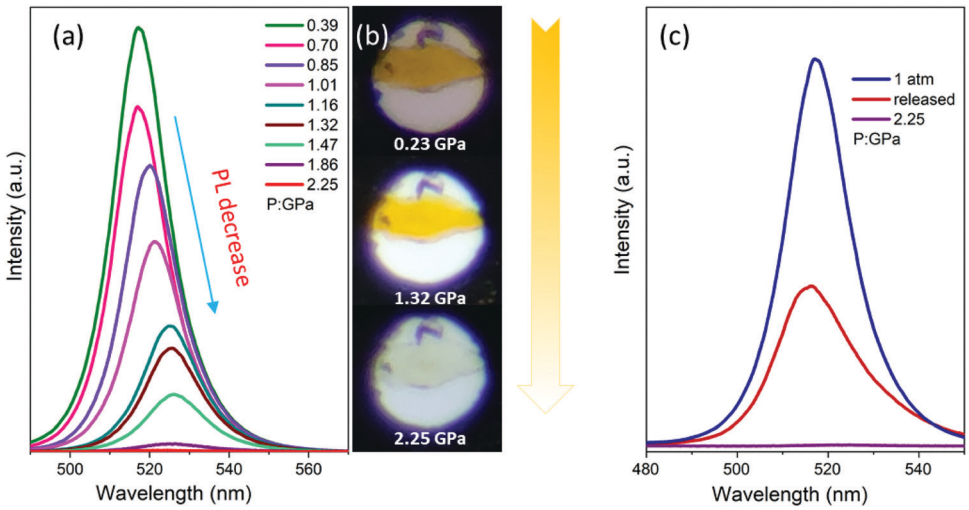

Fig. 2 (a) Pressure-dependent PL spectra of $CsPbBr_3$:Ce QDs excited by a 454 nm laser. (b) Optical micrographs of $CsPbBr_3$:Ce QDs in a diamond anvil cell at selected pressures taken using a stereo microscope. The small dot at the top of the sample is a ruby sphere for pressure calibration. (c) PL spectra at 1 atm during pressurization (blue line), 2.25 GPa (purple line), and 1 atm after depressurization (red line) excited by a 454 nm laser.

2.25 GPa back to 516 nm at 1 atm, indicating that the observed structural phase transition is reversible. Thus the color-changing feature of $CsPbBr_3$:Ce QDs may have potential for applications in optical recording and as pressure sensing materials.

The PL peak energies (E_g) and intensities *vs.* pressure of the $CsPbBr_3$:Ce are plotted in Fig. 3(a) and (b), respectively. In Fig. 3(a), the E_g of $CsPbBr_3$:Ce QDs experiences a continuous narrowing from 2.40 eV under ambient conditions to 2.36 eV at 1.47 GPa before it experiences an abnormal broadening afterwards. The PL intensity of $CsPbBr_3$:Ce QDs experiences a continuous decrease from ambient pressure to 2.25 GPa, while a keen point was observed at 1.47 GPa as shown in Fig. 3(b) which may be associated with pressure induced amorphization, as illustrated above. In Fig. 3(a), the black solid lines represent the results of the least-square fits of the experimental data of E_g *vs.* pressure using a linear function whose pressure coefficients (PCs) are listed in Table 1. The obtained PC, 0.035 eV GPa^{-1}, of $CsPbBr_3$:Ce QDs is slightly smaller than the value of 0.043 eV GPa^{-1} for $CsPbBr_3$ QDs.[26] In Fig. 3(b), the black solid line represents the result of the least-square fits to the experimental data of intensities *vs.* pressure using a linear relation whose PCs are listed in Table 2. The obtained PC of 0.78 a.u. GPa^{-1} for $CsPbBr_3$:Ce QDs is also slightly smaller than the value of 0.86 a.u. GPa^{-1} for $CsPbBr_3$ QDs. This pressure dependence is in perfect agreement with the E_g as a function of pressure.

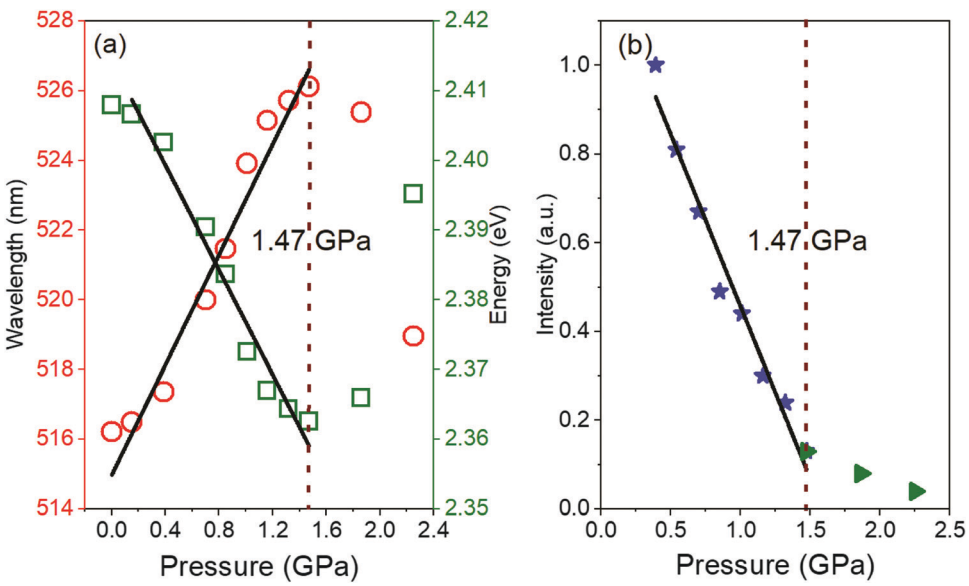

Fig. 3 (a) PL peak location evolutions of $CsPbBr_3$:Ce as a function of pressure. The red circles and the green squares represent the PL peak position and band-gap energy, respectively. (b) The evolution of PL peak intensities of $CsPbBr_3$ as a function of pressure.

Table 1 Coefficients describing the pressure dependence of the PL peaks of $CsPbBr_3$:Ce QDs in the pressure range of 0.39–1.47 GPa obtained from least-square fits to the experimental data displayed in Fig. 3(a) using a linear equation: $E_g = \alpha P + b$

	α (eV GPa^{-1})	b (eV)
0.39–1.47 GPa	-0.035 ± 0.002	2.412 ± 0.002

Table 2 Coefficients describing the pressure dependence of the PL intensities of $CsPbBr_3$:Ce QDs in the pressure range of 0.39–1.47 GPa obtained from least-square fits to the experimental data displayed in Fig. 3(b) using a linear equation: $E_i = nP + m$

	n (a.u. GPa^{-1})	m (a.u.)
0.39–1.47 GPa	-0.777 ± 0.051	1.232 ± 0.051

In order to investigate the band-edge PL kinetics, we conducted TRPL measurements based on time-correlated single photon counting. To figure out the evolution of luminescence lifetime with pressure, the PL decay curves of $CsPbBr_3$:Ce QDs were described with a bi-exponential function after deconvolution. Typical TRPL decay profiles at selected pressures are shown in Fig. 4(a). An abnormal change of the PL decay profile is observed at 1.86 GPa, which is associated with the pressure induced amorphization. Upon decompression, the transient PL decay profile was recovered, indicating that the pressure induced amorphization is reversible. The pressure dependence of lifetime is in good accordance with the conclusion deduced from the steady-state spectrum above and suggests that the nature of the dominant charge carriers is sensitive to the pressure induced phase transition. As shown in Fig. 4(b), the lifetime *vs.* pressure curve of $CsPbBr_3$:Ce demonstrates that the average lifetime (τ) decreases monotonically with increasing pressure. The red solid line represents the result of the least-square fits to the experimental data using a linear function: $\tau = \alpha P + \beta$, and the obtained parameters are $\alpha = -2.76 \pm 0.14$ ns GPa^{-1} and $\beta = 8.41 \pm 0.15$ ns. Based on this fitting, the obtained PL lifetimes are determined to be 7.90 ns at 0.23 GPa and 3.42 ns at 1.86 GPa, while the corresponding variation is about 57%.

The short lifetime (τ_1) and the long lifetime (τ_2) were obtained and are shown in Fig. 4(b). τ_1 can be attributed to the direct radiative transition of the edge excited states, while τ_2 corresponds to the recombination of localized charge carriers at the surface, which is governed by non-radiative processes involving the surface defect states of the QDs. The decreased τ_1 from ambient to 1.86 GPa is caused by the increased overlapping of the exciton wave functions with pressure elevation.[31] On the other hand pressure also facilitates nonradiative electron–hole coupling, which should be related with the reduction of τ_2 below 1.32 GPa. Upon further compression, τ_2 inverts to positive pressure dependence. The application of pressure to non-radiative processes not only decreases the surface defect states but also creates pressure induced

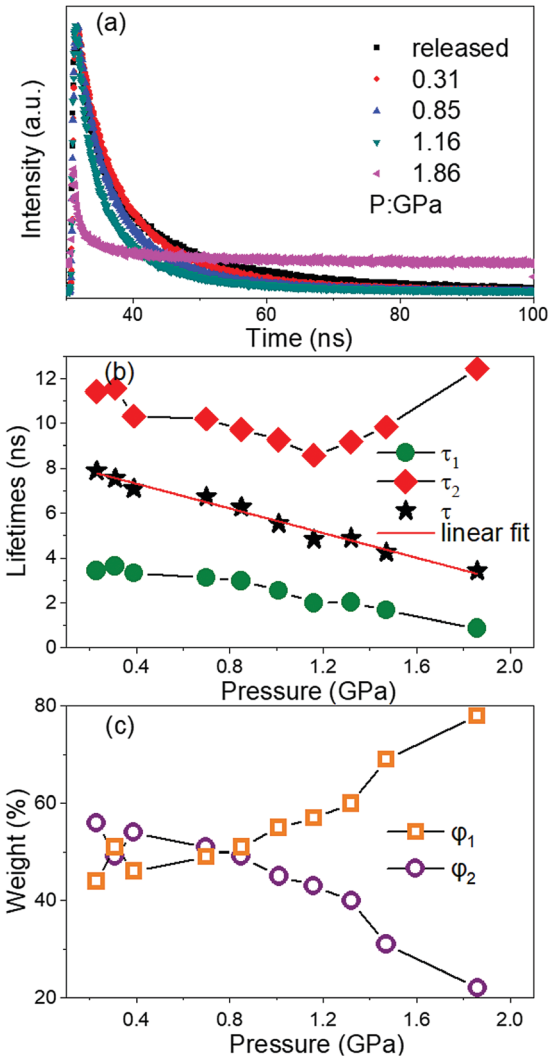

Fig. 4 (a) TRPL decay profiles at selected pressures, with an excitation wavelength of 454 nm. (b) The short lifetime τ_1, long lifetime τ_2, and average lifetime τ of $CsPbBr_3$:Ce QDs as a function of pressure. (c) The corresponding weight φ_1 of short lifetime τ_1 and the weight φ_2 of long lifetime τ_2 as a function of pressure.

structural distortion,[32] which is the primary cause of the positive pressure dependence of τ_2 up to 1.32 GPa. In Fig. 4(c), it is observed that the weight of the long lifetime (φ_2) decreases (from 56% to 22%) with increasing pressure, which is associated with the decrease of the content of the surface defect states. Accordingly, the weight of the short lifetime (φ_1) increases (from 44% to 78%) in the same time. The short lifetime component contributed a larger weight in the decay process, which is an indication of the lifetimes being dominated by recombination of radiative excitation. The general equation for the radiative lifetimes of excitons in QDs is[33]

$$\tau_{rad} = \frac{2\pi\varepsilon_0 m_0 c^3}{ne^2\omega^2 f} \quad (1)$$

where ε_0 is the dielectric constant of vacuum, m_0 is the free electron mass, c is the velocity of light, n is the refractive index,

e is the charge of electron, ω is the transition frequency, and f is the oscillator strength given by[34]

$$f = \frac{E_P}{\hbar\omega}|\psi_h|\psi_e|^2 \quad (2)$$

where E_P is the Kane energy. Thus, eqn (1) can be rewritten as

$$\tau_{rad} = \frac{2\pi\hbar\varepsilon_0 m_0 c^3}{ne^2\omega E_P|\psi_h|\psi_e|^2} \quad (3)$$

As given in eqn (3), the relation between the pressure and the PL lifetimes of QDs is based on the impact of pressure on n, ω, E_P and $|\psi_h|\psi_e|^2$. Thus the relation is complicated but revealed through our experimental results and the literature: (1) the n of bulk $CsPbBr_3$ has a negative PC, while the pressure induced bandgap or size changes play a negligible role in the refractive index;[35] (2) according to Fig. 1(c), the red-shift of the PL peak energy ($\hbar\omega$) results in an increase of $\sim$2% in the PL lifetimes at 1.86 GPa; (3) although no direct research on the pressure dependence of E_P of $CsPbBr_3$ has been reported so far, the E_P only shows a 5% fluctuation with halide substitution of Cl ions based on previous work.[36] In this point of view, the E_P of $CsPbBr_3$ is not sensitive to external factors and has a limited contribution to the variation of PL lifetimes under pressure; (4) owing to the difference between the PCs of bulk $CsPbBr_3$ and $CsPbBr_3$:Ce QDs, the confinement for the carriers in QDs shows a drastically different behavior under compression that it is enhanced by pressure elevation. This enhancement would lead to an increase of the overlap integral of $|\psi_h|\psi_e|^2$, which plays a dominant role in the decrease of PL lifetimes under pressure.

As compared with the report on the pressure evolution of the PL kinetics of $CsPbBr_3$ QDs by Xiao *et al.*, a completely distinct result was revealed in our experiment. Xiao *et al.* reported that at elevated pressures $CsPbBr_3$ experiences a red-shift in PL wavelength with pressure in $CsPbBr_3$ QDs, followed by an increase in lifetimes, but on the contrary we observed an opposite trend with increasing pressure that the lifetimes of $CsPbBr_3$:Ce QDs are reduced with the red-shift in PL wavelength. The lifetime of $CsPbBr_3$:Ce QDs is found to be dependent on pressure with the radiative and non-radiative dynamics, which can be ascribed to the relaxation between bands as well as that between the defect and trap states of the QDs. With increasing pressure, the wave-function overlapping of the excitons is increased, while the surface traps are reduced, which contributed to the decrease of lifetime. In addition, Ce^{3+} doping also contributed to the increase of the near band-edge state density and enhancing the radiative transition of $CsPbBr_3$:Ce QDs, which contribute to the decrease of lifetime.[19] Therefore, the coincident effect of the increasing pressure and the doping of Ce^{3+} cations is responsible for the drastic decrease of lifetime in $CsPbBr_3$:Ce QDs. The ultrafast luminescence decay in the nanosecond range is important to scintillation applications, such as enabling the dynamic real-time X-ray imaging and significantly shortening the dead time for radio detection devices.

4. Conclusion

In summary, we report the $CsPbBr_3$:Ce QDs by the modulated colloidal chemistry method under ambient conditions and tune their PL kinetics through high pressure. Notably, the $CsPbBr_3$:Ce QDs showed smaller PC of intensity and PC of E_g than those of $CsPbBr_3$ QDs. The pressure-modulated PL kinetics of $CsPbBr_3$:Ce QDs were methodically studied with TRPL. A completely distinct result compared to previous studies was observed that the lifetimes of $CsPbBr_3$:Ce QDs were adversely shortened with increasing pressure. These findings significantly deepen the understanding of the PL kinetics of $CsPbBr_3$:Ce QDs under high pressure and will help in broadening the application of optical devices of inorganic perovskite materials in the future.

Conflicts of interest

There are no conflicts to declare.

Acknowledgements

This work was supported by the National Natural Science Foundation of China (Grant No. 11304034 and 11804047), the Science and Technology Development Program of Jilin City (Grant No. 201831733), and Scientific Research Staring Foundation for the Doctors of the Northeast Electric Power University (No. BSJXM-2018223).

References

1 L. Protesescu, S. Yakunin, M. I. Bodnarchuk, F. Krieg, R. Caputo, C. H. Hendon, R. X. Yang, A. Walsh and M. V. Kovalenko, *Nano Lett.*, 2015, **15**, 3692–3696.
2 S. Wei, Y. Yang, X. Kang, L. Wang, L. Huang and D. Pan, *Chem. Commun.*, 2016, **52**, 7265–7268.
3 K. Lin, J. Xing, L. N. Quan, F. P. G. de Arquer, X. Gong, J. Lu, L. Xie, W. Zhao, D. Zhang, C. Yan, W. Li, X. Liu, Y. Lu, J. Kirman, E. H. Sargent, Q. Xiong and Z. Wei, *Nature*, 2018, **562**, 245–248.
4 S. Bade, X. Shan, P. T. Hoang, J. Li, T. Geske, L. Cai, Q. Pei, C. Wang and Z. Yu, *Adv. Mater.*, 2017, **29**, 1607053.
5 Y. Wang, X. Li, J. Song, L. Xiao and H. Sun, *Adv. Mater.*, 2016, **47**, 7101–7108.
6 Q. Han, Y. T. Hsieh, L. Meng, J. L. Wu, P. Y. Sun, E. P. Yao, S. Y. Chang, S. H. Bae, T. Kato, V. Bermudez and Y. Yang, *Science*, 2018, **361**, 904–908.
7 C. X. Bao, J. Yang, S. Bai, W. D. Xu, Z. B. Yan, Q. Y. Xu, J. M. Liu, W. J. Zhang and F. Gao, *Adv. Mater.*, 2018, **30**, 1803422.
8 J. D. Deng, H. R. Wang, J. Xun, J. X. Wang, X. Y. Yang, W. Shen, M. Li and R. X. He, *Mater. Des.*, 2019, **185**, 108246.
9 F. Alam, K. D. Wegner, S. Pouget, L. Amidani and P. Reiss, *J. Chem. Phys.*, 2019, **151**, 231101.
10 W. Liu, Q. Lin, H. Li, K. Wu and V. I. Klimov, *J. Am. Chem. Soc.*, 2017, **138**, 14954–14961.

11 L. Zhou, T. Liu, J. Zheng, K. Yu, F. Yang, N. Wang, Y. Zuo, Z. Liu, C. Xue and C. Li, *J. Phys. Chem. C*, 2018, **122**, 26825–26834.
12 Y. Fujimoto, K. Saeki, H. Tanaka, T. Yahaba and K. Asai, *Phys. Scr.*, 2016, **91**, 094002.
13 Y. Cheng, C. Shen, L. Shen, W. Xiang and X. Liang, *ACS Appl. Mater. Interfaces*, 2018, **10**, 21434–21444.
14 M. Zeng, F. Artizzu, J. Liu, S. Singh, F. Locardi, D. Mara, Z. Hens and R. VanDeun, *ACS Appl. Nano Mater.*, 2020, **3**, 4699–4707.
15 Y. Xie, B. Peng, I. Bravi, Y. Yu, Y. Dong, R. Liang, Q. Ou, B. Monserrat and S. Zhang, *Adv. Sci.*, 2020, **7**, 2001698.
16 W. Stam, J. J. Guechies, T. Altantzis, K. H. W. Bos, J. D. Meeldijk, S. V. Aert, S. Bals, D. Vanmaekelbergh and C. M. Donega, *J. Am. Chem. Soc.*, 2017, **139**, 4087–4097.
17 S. Zhao, Y. Zhang and Z. Zang, *Chem. Commun.*, 2020, **56**, 5811–5814.
18 F. Liu, C. Ding, Y. H. Zhang, T. S. Ripolles, T. C. Kamisaka, T. Toyoda, S. Hayase, T. Minemoto, K. J. Yoshino and S. Y. Dai, *et al.*, *J. Am. Chem. Soc.*, 2017, **139**, 16708–16719.
19 J. S. Yao, J. Ge, B. N. Han, K. H. Wang, H. B. Yao, H. L. Yu, J. H. Li, B. S. Zhu, J. Z. Song, C. Chen and Q. Zhang, *et al.*, *J. Am. Chem. Soc.*, 2018, **140**, 3626–3634.
20 D. L. Zhou, D. L. Liu, G. C. Pan, X. Chen, D. Y. Li, W. Xu, X. Bai and H. W. Song, *Adv. Mater.*, 2017, **29**, 1704149.
21 H. Li, L. M. He, B. Zhong, Y. Li, S. K. Wu, J. Liu and G. Q. Yang, *ChemPhysChem*, 2010, **5**, 124–127.
22 Y. Shi, Z. W. Ma, D. L. Zhao, Y. P. Chen, Y. Cao, K. Wang, G. J. Xiao and B. Zou, *J. Am. Chem. Soc.*, 2019, **141**, 6504–6508.
23 L. Zhang, Q. X. Zeng and K. Wang, *J. Phys. Chem. Lett.*, 2017, **8**, 3752–3758.
24 L. Zhang, C. M. Liu, L. R. Wang, C. L. Liu, K. Wang and B. Zou, *Angew. Chem., Int. Ed.*, 2018, **130**, 11383–11387.
25 S. Jiang, Y. Fang, R. Li, H. Xiao, J. Crowley, C. Wang, T. J. White, W. A. Goddard, Z. Wang and T. Baikie, *Angew. Chem., Int. Ed.*, 2016, **55**, 6540–6544.
26 G. J. Xiao, Y. Cao, G. G. Qi, L. R. Wang, C. Liu, Z. W. Ma, X. Y. Yang, Y. M. Sui, W. T. Zheng and B. Zou, *J. Am. Chem. Soc.*, 2017, **139**, 10087–10094.
27 G. C. Pan, X. Bai, D. W. Yang, X. Chen, P. T. Jing, S. G. Qu, L. J. Zhang, D. L. Zhou, J. Y. Zhu and W. Xu, *Nano Lett.*, 2017, **17**, 8005–8011.
28 S. H. Zou, Y. S. Liu, J. H. Li, C. P. Liu, R. Feng, F. L. Jiang, Y. X. Li, J. Z. Song, H. B. Zeng, M. C. Hong and X. Y. Chen, *J. Am. Chem. Soc.*, 2017, **139**, 11443–11450.
29 M. D. Wisser, M. Chea, Y. Lin, D. M. Wu, W. L. Mao, A. Salleo and J. A. Dionne, *Nano Lett.*, 2015, **15**, 1891–1897.
30 Z. Guo, X. Wu, T. Zhu, X. Zhu and L. Huang, *ACS Nano*, 2016, **10**, 9992–9998.
31 L. Kong, G. Liu, J. Gong, Q. Hu, R. D. Schaller, P. Dera, D. Zhang, Z. Liu, W. Yang and K. Zhu, *et al.*, *Proc. Natl. Acad. Sci. U. S. A.*, 2016, **113**, 8910–8915.
32 L. Qiao, W. H. Fang, R. Long and O. V. Prezhdo, *J. Am. Chem. Soc.*, 2021, **143**, 9982–9990.
33 G. W. P't Hooft, W. A. J. A. van der Poel, L. W. Molenkamp and C. T. Foxon, *Phys. Rev. B: Condens. Matter Mater. Phys.*, 1987, **35**, 8281–8284.
34 P. Tighineanu, R. Daveau, E. H. Lee, J. D. Song, S. Stobbe and P. Lodahl, *Phys. Rev. B: Condens. Matter Mater. Phys.*, 2013, **88**, 608–613.
35 Z. Yang, J. F. Lu, M. H. Zhuge, Y. Cheng, J. F. Hu, F. T. Li, S. Qiao, Y. F. Zhang, G. F. Hu and Q. Yang, *Adv. Mater.*, 2019, **31**, 1900647.
36 M. A. Be Cker, R. Vaxenburg, G. Nedelcu, P. C. Sercel and A. L. Efros, *Nature*, 2018, **553**, 189–193.